

Chapter 1

Introduction

This chapter starts with an overview of the celestial mechanics. Applications of Restricted Three Body Problem (RTBP), its particular cases and different perturbing forces affecting the motion of the infinitesimal body are reviewed. Equations of motion of the infinitesimal body, the methods of finding halo orbits and the procedure for obtaining Poincaré Surface of Sections (PSS) are also described.

1.1 Overview of celestial mechanics

Celestial mechanics is a branch of astronomy which studies the motion of astronomical bodies by applying the principles of classical mechanics for producing ephemeris data. Orbital mechanics is a subfield of celestial mechanics which deals with the practical problems concerning the motion of rockets and spacecrafts, and plays a pioneer role in space mission design and control. In 1596, Kepler described the model of solar system in the first edition of his book *Mysterium Cosmographicum* according to which planets moved within spherical shells whose inner and outer surfaces had precise separations determined by the circumspheres and inspheres of the regular polyhedra. He had considered six planets in his model. In Fig. 1.1, Kepler's model for outer planets is shown (Murray and Dermott (1999)). According to Kepler, the widths of these shells were related to the orbital eccentricities. Kepler empirically tried to get the simple numerical relationships between the orbital distances of the planets, but couldn't succeed. From the observations made by Tycho Brahe and using his empirical approach, Kepler derived three laws of planetary motion which are

1. The planets move in elliptical orbits around the Sun with the Sun at one focus.
2. A radius vector from the Sun to a planet sweeps out equal areas in equal times.
3. The square of the orbital period of a planet is proportional to the cube of its semi-major axis.

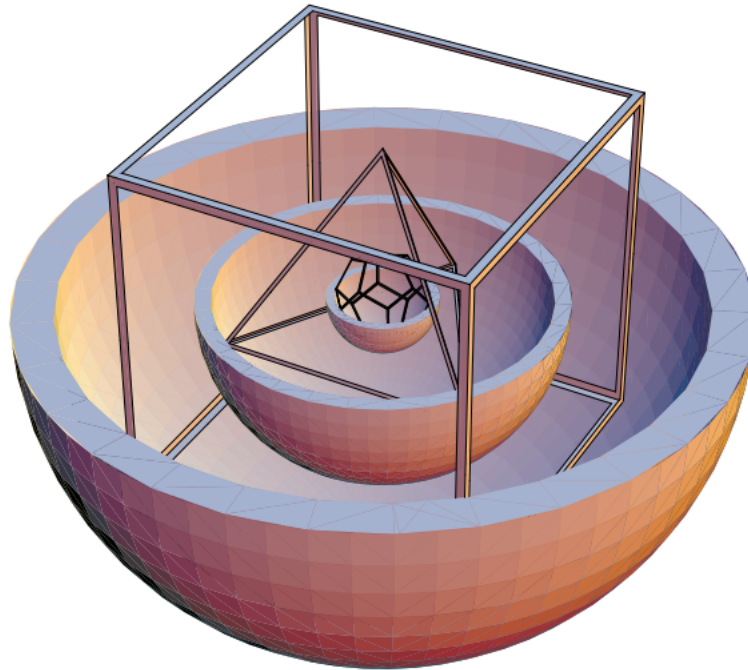


FIGURE 1.1: Kepler's planetary model for outer planets (Adapted from Murray and Dermott (1999))

In the seventeenth century, Newton established that all motion in the solar system results from the inverse square law of force. He could also show that Kepler's three laws of planetary motion can be derived as a consequence of this force and the resulting motion can be described using conic sections. So, Newton unified the celestial and terrestrial dynamics. In celestial mechanics, most of the results are derived by considering the celestial bodies as point masses. Since the celestial bodies are assumed to be spherical and the size of these objects are negligible compared to the distances between them, it is possible to treat these objects as point masses. So, the study of the motion of two spherical bodies under their mutual gravitational attraction reduces to the study of the motion of two point masses under their mutual gravitation attraction. This is called the two body problem. Newton was the first to solve the two body problem. He obtained the solution using the geometric method. The analytic solution was given by Bernoulli, which was investigated by Euler.

1.2 Restricted Three Body Problem

Two-body problem can be used to study the motion of two rigid bodies orbiting each other under the influence of mutual gravitational attraction. For example, the motion of a planet orbiting a star or motion of binary stars orbiting around their barycentre can be analyzed using the two-body problem.

After solving the two-body problem, Newton focused on more complex systems containing three participating bodies but could not attain much success. After Newton, many researchers tried to solve the three body problem. But no one could obtain a closed form solution. In general, N -body problem does not have a closed form solution for $N \geq 3$. Different particular solutions of three body problem exist. One such solution was suggested by Euler in 1765. He assumed the three masses to be collinear. In the case of equal masses, two bodies rotate in circles around the third. For unequal masses, each mass will travel in elliptical orbit around the center of mass. A drawback of this model is that the orbit is unstable under small perturbations.

The model suggested by Lagrange in 1772 consists of three masses situated at the vertices of an equilateral triangle. If the three masses are equal, all three bodies trace the same circular orbit. If the masses are different, they will follow elliptical orbit still remaining at the vertices of the equilateral triangle. If one of the masses completely dominates the other masses, then the solution becomes stable. Another particular solution, known as Figure-Eight solution, discovered by Christopher Moore in 1993 was a numerical solution which occurs only when the masses are equal. The center of mass of the system being at the cross point. This model gives a stable solution. In the Hill's solution, two of the masses remain close to each other forming a binary and they together orbit the third body which is farther away like Sun-Earth-Moon system.

Euler was the first one to propose restricted three body problem, a simplified three body problem. The Restricted Three Body Problem (RTBP) deals with the motion of an infinitesimal body which moves under the gravitational influence of two massive bodies called the primaries. The mass of the infinitesimal body is so negligible compared to the masses of the primaries that it does not influence the motion of the primaries. In solar system, the masses of many celestial bodies like natural satellites, asteroids, comets, etc. are negligible compared to the masses of the planets and stars. So, RTBP can be used to study the motion of such celestial bodies. Further, the motion of planets around the Sun is almost circular which suggests the concept of Circular Restricted Three Body Problem (CRTBP), a particular case of RTBP, in which the primaries move in circular orbits around each other. Another particular case of RTBP is Elliptical Restricted Three Body Problem (ERTBP) in which the primaries are assumed to move in elliptic orbits around their barycentre.

Significant contributions in CRTBP came from the works of two great mathematicians Lagrange and Jacobi. Lagrange discovered five equilibrium points known as Lagrangian points. Jacobi considered CRTBP in the synodic coordinate system and evaluated the first integral of equations of motion, which is the only constant in CRTBP. This constant is known as the Jacobi constant.

In solar system, the infinitesimal body experiences forces other than the gravitational force of the primaries. Such forces are called perturbing forces. Solar radiation pressure force, force due to oblate primary, Poynting-Robertson force, atmospheric drag, etc. are examples perturbing forces. The perturbations due to radiation and oblateness of the primaries are considered in this study. In 1891, with the help of experiments the Russian physicist Pyotr Nikolayevich Lebedev proved that light exerts a mechanical pressure on material bodies and gave the following law (Pathak (2017)):

“The minute pressure exerted by radiation on bodies is inversely proportional to the square of the distance between the light source and the illuminated body.”

Since then many researchers have considered the perturbing force due to radiation of the primaries in the study of RTBP. The force due to radiation of the primary can be divided into three components: the radiation pressure, the Doppler shift of the incident radiation and the Poynting drag. Radzievskii (1950) showed that the effect of the Doppler shift of the incident radiation and the Poynting drag is negligible compared to the radiation pressure. The radiation pressure force (F_p) varies with the distance in a similar way as the gravitational force (F_g) varies but acts in the opposite direction. Then the resultant force exerted by the radiating body on the infinitesimal body is

$$F = F_g - F_p = \left(1 - \frac{F_p}{F_g}\right)F_g = qF_g,$$

where $q = 1 - (F_p/F_g)$. The factor q reduces the effective mass of the radiating body, hence it is called the mass reduction factor. If the primary is not radiating, then $F_p = 0$, so $q = 1$. In the Sun-Planet systems, $q \approx 1$ as $F_g \gg F_p$. Researchers have computed equilibrium points and studied their stability in the CRTBP and ERTBP by considering one or both the primaries as a source of radiation (Rabe (1973), Sharma (1987), Meire (1981), Zimovshchikov and Tkhai (2004), Kumar and Narayan (2012), Narayan and Kumar (2011), Narayan and Singh (2014), Singh and Narayan (2015), Rahoma et al. (2019), Roberts (2002), Jorba-Cusco et al. (2021), and Singh and Tyokyaa (2023)).

In classical RTBP, the primaries are considered to be perfect spheres. But in solar

system, many celestial bodies bulges out at equator and are flatted at the poles due to rotation about their axis. An oblate spheroid provides good approximation for such deformed celestial bodies. The oblateness coefficient of a celestial body is denoted by A and it is defined as

$$A = \frac{R_e^2 - R_p^2}{5R^2},$$

where R_e and R_p , respectively, are the equatorial and polar radii of the object and R is the distance between the primaries. Abouelmagd (2013) has considered the motion of infinitesimal body in CRTBP by considering both the primaries radiating and oblate. The author has considered different perturbed cases and analyzed the motion in each case. Various authors have studied RTBP by considering oblateness of the primaries (Sharma and Subba Rao (1979), Subba Rao and Sharma (1996), Markellos et al. (1996), AbdulRaheem and Singh (2006), Abouelmagd et al. (2013), and Ansari et al. (2019)).

1.3 Equations of motion

In this section, the equations of motion of an infinitesimal body in a dimensionless synodic coordinate system in CRTBP and ERTBP framework are given. Suppose m_1 and m_2 ($m_1 > m_2$) are masses of primaries P_1 and P_2 , respectively, and m is the mass of the infinitesimal body. A schematic diagram of Restricted Three Body Problem is given in Fig. 1.2. The mass factor or mass ratio of the primaries is denoted by μ and it is defined as $\mu = m_2/(m_1 + m_2)$.

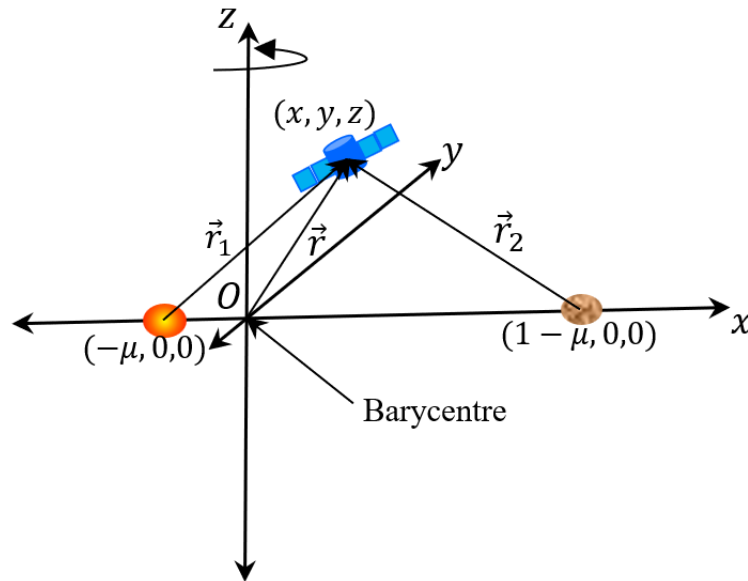


FIGURE 1.2: Schematic diagram of RTBP in a dimensionless synodic coordinate system

1.3.1 Equations of motion in CRTBP framework

Suppose the primaries P_1 and P_2 are moving in circular orbits around their barycentre and the infinitesimal body is free to move in space. Now, consider a sidereal coordinate system XYZ such that its origin is at the barycentre of the primaries and its XY plane coincides with the plane of motion of the primaries. Then the primaries P_1 and P_2 will always remain in the XY plane. Suppose $(X_1, Y_1, 0)$ and $(X_2, Y_2, 0)$ are coordinates of primaries P_1 and P_2 , respectively, and the infinitesimal body is located at (X, Y, Z) . Here, both the primaries are assumed to be source of radiation and oblate spheroids. Then the motion of the infinitesimal body in the sidereal system is given by

$$\begin{aligned}\ddot{X} &= \frac{\partial U_1}{\partial X}, \\ \ddot{Y} &= \frac{\partial U_1}{\partial Y}, \\ \ddot{Z} &= \frac{\partial U_1}{\partial Z},\end{aligned}\tag{1.1}$$

where

$$U_1 = k^2 \left(\frac{m_1 q_1}{R_1} + \frac{m_1 q_1 A_1}{2R_1^3} + \frac{m_2 q_2}{R_2} + \frac{m_2 q_2 A_2}{2R_2^3} \right),\tag{1.2}$$

$$\begin{aligned}R_1 &= \sqrt{(X - X_1)^2 + (Y - Y_1)^2 + Z^2}, \\ R_2 &= \sqrt{(X - X_2)^2 + (Y - Y_2)^2 + Z^2}.\end{aligned}\tag{1.3}$$

Here, an overhead dot denotes a differentiation with respect to time t^* , k^2 is universal gravitational constant, q_i and A_i , respectively, are mass reduction factors and oblateness coefficients of primaries, $i = 1, 2$ and R_i is the distance between the i^{th} ($i = 1, 2$) primary and the infinitesimal body. Now, the coordinate system XYZ is rotated through an angle nt^* about z -axis so that the primaries always lie on the \tilde{X} -axis of the new coordinate system $\tilde{X}\tilde{Y}\tilde{Z}$. The transformation between the two coordinate frames is given by (Szebehely (1967, p.14))

$$\begin{aligned}X &= \tilde{X} \cos nt^* - \tilde{Y} \sin nt^*, \\ Y &= \tilde{X} \sin nt^* + \tilde{Y} \cos nt^*, \\ Z &= \tilde{Z}.\end{aligned}$$

Then system (1.1) gets transformed to

$$\begin{aligned}\ddot{\tilde{X}} - 2n\dot{\tilde{Y}} &= \frac{\partial U_1}{\partial \tilde{X}}, \\ \ddot{\tilde{Y}} + 2n\dot{\tilde{X}} &= \frac{\partial U_1}{\partial \tilde{Y}}, \\ \ddot{\tilde{Z}} &= \frac{\partial U_1}{\partial \tilde{Z}},\end{aligned}\tag{1.4}$$

where U_1 is as in (1.2) and

$$\begin{aligned}R_i^2 &= (\tilde{X} - \tilde{X}_i)^2 + \tilde{Y}^2 + \tilde{Z}^2, \quad i = 1, 2, \\ \tilde{X}_1 &= -\frac{m_2}{m_1 + m_2}l, \quad \tilde{X}_2 = \frac{m_1}{m_1 + m_2}l.\end{aligned}\tag{1.5}$$

Here, l is the constant distance between the two primaries. Next, the synodic frame $\tilde{X}\tilde{Y}\tilde{Z}$ is transformed to a dimensionless synodic frame xyz using the transformations (Szebehely (1967, p.16))

$$\begin{aligned}x &= \frac{\tilde{X}}{l}, \quad y = \frac{\tilde{Y}}{l}, \quad z = \frac{\tilde{Z}}{l}, \quad x_1 = \frac{\tilde{X}_1}{l}, \quad x_2 = \frac{\tilde{X}_2}{l}, \quad r_1 = \frac{R_1}{l}, \quad r_2 = \frac{R_2}{l}, \quad t = nt^*, \\ \mu &= \frac{m_2}{m_1 + m_2}, \quad 1 - \mu = \frac{m_1}{m_1 + m_2}.\end{aligned}$$

Then in the coordinate system xyz , the primaries P_1 and P_2 always remain fixed on the x -axis at $(-\mu, 0, 0)$ and $(1 - \mu, 0, 0)$, respectively, and equations of motion of infinitesimal body are given by (Abouelmagd (2013))

$$\begin{aligned}\ddot{x} - 2n\dot{y} &= \Omega_x^*, \\ \ddot{y} + 2n\dot{x} &= \Omega_y^*, \\ \ddot{z} &= \Omega_z^*,\end{aligned}\tag{1.6}$$

where

$$\Omega^* = \frac{1}{2}n^2(x^2 + y^2) + \frac{(1 - \mu)q_1}{r_1} + \frac{(1 - \mu)q_1A_1}{2r_1^3} + \frac{\mu q_2}{r_2} + \frac{\mu q_2A_2}{2r_2^3}\tag{1.7}$$

and

$$n^2 = 1 + \frac{3}{2}(A_1 + A_2),\tag{1.8}$$

$$r_1 = \sqrt{(x + \mu)^2 + y^2 + z^2},\tag{1.8}$$

$$r_2 = \sqrt{(x + \mu - 1)^2 + y^2 + z^2}.\tag{1.9}$$

The quantity Ω^* is pseudo potential; n is the mean motion and r_i is the distance between the i^{th} ($i = 1, 2$) primary and the infinitesimal body.

1.3.2 Equations of motion in ERTBP framework

Assume that the primaries are moving in elliptic orbits around their barycentre and the infinitesimal body can move in space. Consider a sidereal coordinate system XYZ whose origin lies at the barycentre of the primaries and its XY plane is the plane of motion of the primaries. The primaries P_1 and P_2 are located at $(X_1, Y_1, 0)$ and $(X_2, Y_2, 0)$, respectively and the infinitesimal body is located at (X, Y, Z) in this sidereal system. Suppose both the primaries are source of radiation. Then the equations of motion of the infinitesimal body are given by

$$\begin{aligned}\ddot{X} &= \frac{\partial U_2}{\partial X}, \\ \ddot{Y} &= \frac{\partial U_2}{\partial Y}, \\ \ddot{Z} &= \frac{\partial U_2}{\partial Z},\end{aligned}\tag{1.10}$$

where

$$U_2 = k^2 \left(\frac{m_1 q_1}{R_1} + \frac{m_2 q_2}{R_2} \right),\tag{1.11}$$

$$\begin{aligned}R_1 &= \sqrt{(X - X_1)^2 + (Y - Y_1)^2 + Z^2}, \\ R_2 &= \sqrt{(X - X_2)^2 + (Y - Y_2)^2 + Z^2}.\end{aligned}\tag{1.12}$$

Here, an overhead dot denotes a differentiation with respect to time t^* , k^2 is universal gravitational constant, q_i are mass reduction factors of primaries, $i = 1, 2$ and R_i is the distance between the i^{th} ($i = 1, 2$) primary and the infinitesimal body. Now, the coordinate system is rotated through an angle θ , the true anomaly of P_1 , about Z axis so that the primaries always lie on the new X -axis, \tilde{X} , in the rotating frame. The relation between the old XYZ and the new $\tilde{X}\tilde{Y}\tilde{Z}$ coordinate system is given by (Szebehely (1967))

$$\begin{aligned}X &= \tilde{X} \cos \theta - \tilde{Y} \sin \theta, \\ Y &= \tilde{X} \sin \theta + \tilde{Y} \cos \theta, \\ Z &= \tilde{Z}.\end{aligned}$$

Using above transformation in system (1.10), the equations of motion get transformed to (Szebehely (1967) and Ammar (2008))

$$\begin{aligned}\ddot{\tilde{X}} - 2\dot{\tilde{Y}}\dot{\theta} - \dot{\theta}^2\tilde{X} - \ddot{\theta}\tilde{Y} &= \frac{\partial U_2}{\partial \tilde{X}}, \\ \ddot{\tilde{Y}} + 2\dot{\tilde{X}}\dot{\theta} - \dot{\theta}^2\tilde{Y} + \ddot{\theta}\tilde{X} &= \frac{\partial U_2}{\partial \tilde{Y}}, \\ \ddot{\tilde{Z}} &= \frac{\partial U_2}{\partial \tilde{Z}},\end{aligned}\tag{1.13}$$

where U_2 is as in (1.11) and

$$\begin{aligned}R_i^2 &= (\tilde{X} - \tilde{X}_i)^2 + \tilde{Y}^2 + \tilde{Z}^2, \quad i = 1, 2, \\ \tilde{X}_1 &= -\frac{m_2}{m_1 + m_2}R, \quad \tilde{X}_2 = \frac{m_1}{m_1 + m_2}R.\end{aligned}\tag{1.14}$$

Here, R is the variable distance between the two primaries. Next, the synodic frame $\tilde{X}\tilde{Y}\tilde{Z}$ is transformed to a dimensionless pulsating synodic frame xyz using the transformations (Szebehely (1967, p.16))

$$\begin{aligned}x &= \frac{\tilde{X}}{R}, \quad y = \frac{\tilde{Y}}{R}, \quad z = \frac{\tilde{Z}}{R}, \quad x_1 = \frac{\tilde{X}_1}{R}, \quad x_2 = \frac{\tilde{X}_2}{R}, \quad r_1 = \frac{R_1}{R}, \quad r_2 = \frac{R_2}{R}, \\ \mu &= \frac{m_2}{m_1 + m_2}, \quad 1 - \mu = \frac{m_1}{m_1 + m_2}.\end{aligned}$$

The equations of motion in the dimensionless pulsating synodic coordinate system are (Szebehely (1967))

$$\begin{aligned}\frac{d^2x}{d\theta^2} - 2\frac{dy}{d\theta} &= \frac{1}{1 + e \cos \theta}\Omega_x, \\ \frac{d^2y}{d\theta^2} + 2\frac{dx}{d\theta} &= \frac{1}{1 + e \cos \theta}\Omega_y, \\ \frac{d^2z}{d\theta^2} + z &= \frac{1}{1 + e \cos \theta}\Omega_z,\end{aligned}\tag{1.15}$$

where

$$\begin{aligned}\Omega &= \frac{1}{2}(x^2 + y^2 + z^2) + \frac{(1 - \mu)q_1}{r_1} + \frac{\mu q_2}{r_2}, \\ r_1 &= \sqrt{(x + \mu)^2 + y^2 + z^2}, \\ r_2 &= \sqrt{(x + \mu - 1)^2 + y^2 + z^2}.\end{aligned}\tag{1.16}$$

Here, θ , the true anomaly of P_1 , is the independent variable instead of time t^* , Ω is pseudo potential function, q_1 and q_2 are mass reduction factors of P_1 and P_2 , respectively and r_i ($i = 1, 2$) are as defined earlier.

Now, consider the eccentric anomaly, say E , corresponding to true anomaly θ . The conservation of angular momentum $h = R^2\dot{\theta}$ (Murray and Dermott (1999, p.25)) gives

$$\frac{d\theta}{dt} = \frac{\sqrt{a(1-e^2)}}{R^2}, \quad (1.17)$$

where $R = a(1 - e \cos E)$ is the variable distance between the primaries, a and e , respectively, are semimajor axis and the eccentricity of the orbit of the primaries.

The differential relation between t and E are given by (Danby (1962, p.131))

$$dt = a^{3/2}(1 - e \cos E)dE. \quad (1.18)$$

Using equation (1.18) in (1.17), the differential relation between θ and E can be obtained as

$$d\theta = \frac{\sqrt{a(1-e^2)}}{R^2} a^{3/2}(1 - e \cos E)dE = \frac{a\sqrt{1-e^2}}{R} dE$$

which can be expressed as

$$\frac{dE}{d\theta} = \frac{\rho}{\sqrt{1-e^2}}, \quad (1.19)$$

where $\rho = R/a$. Thus,

$$\frac{d(\cdot)}{d\theta} = \frac{dE}{d\theta} \frac{d(\cdot)}{dE} \quad (1.20)$$

and

$$\begin{aligned} \frac{d^2(\cdot)}{d\theta^2} &= \frac{d}{d\theta} \left(\frac{d(\cdot)}{d\theta} \right) = \frac{d}{dE} \left(\frac{dE}{d\theta} \frac{d(\cdot)}{dE} \right) \frac{dE}{d\theta}, \\ &= \frac{\rho^2}{1-e^2} \frac{d^2(\cdot)}{dE^2} + \frac{\rho}{\sqrt{1-e^2}} \left[\frac{d}{dE} \left(\frac{\rho}{\sqrt{1-e^2}} \right) \right] \frac{d(\cdot)}{dE} \end{aligned}$$

which simplifies to

$$\frac{d^2(\cdot)}{d\theta^2} = \frac{\rho^2}{1-e^2} \frac{d^2(\cdot)}{dE^2} + \frac{\rho}{1-e^2} e \sin E \frac{d(\cdot)}{dE}. \quad (1.21)$$

Using expressions (1.20) and (1.21) in system (1.15), we get

$$\begin{aligned} x'' + \frac{e \sin E}{\rho} x' - \frac{2\sqrt{1-e^2}}{\rho} y' &= \frac{\partial \Omega^*}{\partial x}, \\ y'' + \frac{e \sin E}{\rho} y' + \frac{2\sqrt{1-e^2}}{\rho} x' &= \frac{\partial \Omega^*}{\partial y}, \\ z'' + \frac{e \sin E}{\rho} z' &= \frac{\partial \Omega^*}{\partial z}, \end{aligned} \quad (1.22)$$

where ' denotes the derivative with respect to E ,

$$\Omega^* = \frac{1}{\rho} \left[\frac{1}{2}(x^2 + y^2) - \frac{e}{2\rho}(\cos E - e)z^2 + \frac{(1-\mu)q_1}{r_1} + \frac{\mu q_2}{r_2} \right].$$

The pseudo potential function is an explicit function of eccentric anomaly. Averaging Ω^* with respect to E over the interval 0 to 2π , the averaged pseudo potential function, $\bar{\Omega}$ will be

$$\bar{\Omega} = \frac{1}{2\pi} \int_0^{2\pi} \Omega^* dE = \frac{1}{\sqrt{1-e^2}} \left[\frac{1}{2}(x^2 + y^2) + \frac{(1-\mu)q_1}{r_1} + \frac{\mu q_2}{r_2} \right], \quad (1.23)$$

which does not contain independent variable explicitly. Averaging the coefficients of the first equation of system (1.22),

$$\begin{aligned} & \frac{1}{2\pi} \int_0^{2\pi} \left(x'' + \frac{e \sin E}{\rho} x' - \frac{2\sqrt{1-e^2}}{\rho} y' \right) dE \\ &= \frac{1}{2\pi} x'' \int_0^{2\pi} dE + \frac{e}{2\pi} x' \int_0^{2\pi} \frac{e \sin E}{\rho} dE - \frac{2\sqrt{1-e^2}}{2\pi} y' \int_0^{2\pi} \frac{1}{\rho} dE \\ &= x'' + 0 - \frac{2\sqrt{1-e^2}}{2\pi} y' \left(\frac{2\pi}{\sqrt{1-e^2}} \right) \\ &= x'' - 2y'. \end{aligned}$$

Similarly, averaging the coefficients of the second and the third equations of system (1.22), the new system governing the motion of infinitesimal body has following form:

$$\begin{aligned} x'' - 2y' &= \frac{\partial \bar{\Omega}}{\partial x}, \\ y'' + 2x' &= \frac{\partial \bar{\Omega}}{\partial y}, \\ z'' &= \frac{\partial \bar{\Omega}}{\partial z}, \end{aligned} \quad (1.24)$$

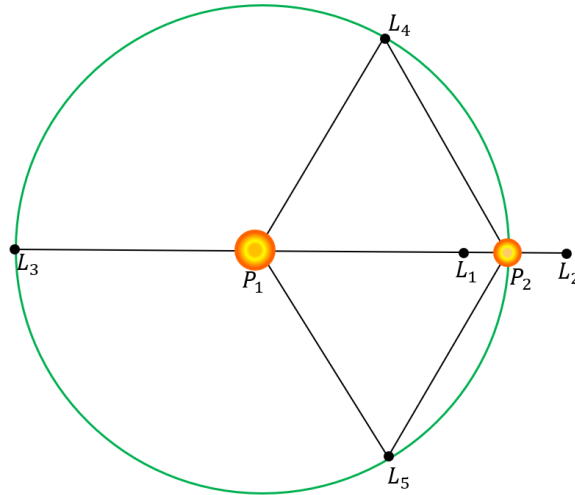


FIGURE 1.3: Lagrangian points in classical RTBP

where

$$\begin{aligned} \bar{\Omega} &= \frac{1}{\sqrt{1-e^2}} \left[\frac{1}{2}(x^2 + y^2) + \frac{(1-\mu)q_1}{r_1} + \frac{\mu q_2}{r_2} \right], \\ r_1 &= \sqrt{(x+\mu)^2 + y^2 + z^2}, \\ r_2 &= \sqrt{(x+\mu-1)^2 + y^2 + z^2}. \end{aligned} \quad (1.25)$$

Equations (1.24) represent the motion of infinitesimal body in a dimensionless synodic coordinate system with eccentric anomaly as independent variable.

1.4 Lagrangian points

Lagrangian points or libration points are equilibrium points of RTBP. These are the locations in the space where the infinitesimal body experiences the balance between the gravitational pull of the primaries, centrifugal force and all other perturbing forces. At Lagrangian points, the infinitesimal body has zero velocity and zero acceleration and therefore, it can maintain its position without much fuel consumption. A RTBP has five planar Lagrangian points which are denoted by L_1, L_2, \dots, L_5 . Out of these five Lagrangian points, three Lagrangian points, L_1, L_2 and L_3 lie on the line joining the primaries and they are called collinear Lagrangian points. The Lagrangian point L_1 lies between the two primaries, L_2 lies on the right side of the second primary P_2 and L_3 lies on the left side of the primary P_1 and always remains hidden behind it. Remaining two Lagrangian points are called triangular Lagrangian points and they lie on the opposite sides of the line joining the primaries. In the classical RTBP, these two points form equilateral triangles with the primaries which are shown in Fig. 1.3.

1.4.1 Computation of collinear Lagrangian points in CRTBP

Location of Lagrangian points can be obtained by solving three simultaneous equations

$$\Omega_x^* = 0, \quad \Omega_y^* = 0, \quad \Omega_z^* = 0.$$

From equations (1.6), we get,

$$n^2 x - \frac{(1-\mu)q_1(x+\mu)}{r_1^3} - \frac{3(1-\mu)q_1 A_1(x+\mu)}{2r_1^5} - \frac{\mu q_2(x+\mu-1)}{r_2^3} - \frac{3\mu q_2 A_2(x+\mu-1)}{2r_2^5} = 0, \quad (1.26)$$

$$y \left[n^2 - \frac{(1-\mu)q_1}{r_1^3} - \frac{3(1-\mu)q_1 A_1}{2r_1^5} - \frac{\mu q_2}{r_2^3} - \frac{3\mu q_2 A_2}{2r_2^5} \right] = 0, \quad (1.27)$$

$$z \left[\frac{(1-\mu)q_1}{r_1^3} + \frac{3(1-\mu)q_1 A_1}{2r_1^5} + \frac{\mu q_2}{r_2^3} + \frac{3\mu q_2 A_2}{2r_2^5} \right] = 0. \quad (1.28)$$

From equation (1.28), we get $z = 0$ which shows all Lagrangian points lie in a plane. For getting collinear Lagrangian points, we must have $y = z = 0$ in (1.26). Suppose the Lagrangian point L_i is located at $(x_i, 0, 0)$, $i = 1, 2, 3$ and γ is the distance between the Lagrangian point and the nearest primary.

Location of L_1

In this case, P_2 is the nearest primary to L_1 . Then since P_1 is located at $(-\mu, 0, 0)$ and P_2 is located at $(1-\mu, 0, 0)$, from Fig. 1.4,

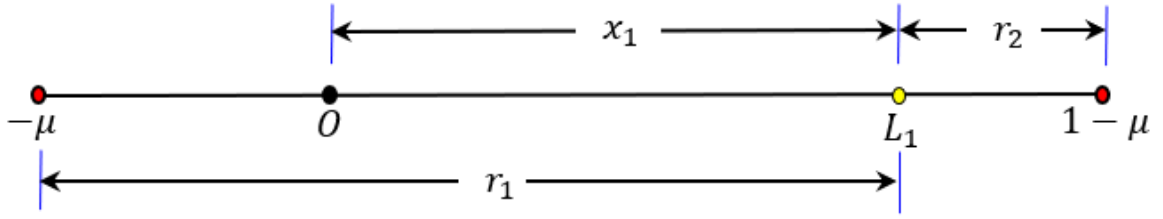
$$r_1 = x_1 + \mu, \quad r_2 = 1 - \mu - x_1.$$

Since γ is the distance between L_1 and P_2 and the distance between the primaries is unity, we have

$$x_1 = 1 - \mu - \gamma, \quad r_1 = 1 - \gamma, \quad r_2 = \gamma. \quad (1.29)$$

Using equation (1.29) in (1.26), we get

$$n^2(1 - \mu - \gamma) - \frac{(1-\mu)q_1}{(1-\gamma)^2} - \frac{3(1-\mu)q_1 A_1}{2(1-\gamma)^4} + \frac{\mu q_2}{\gamma^2} + \frac{3\mu q_2 A_2}{2\gamma^4} = 0$$

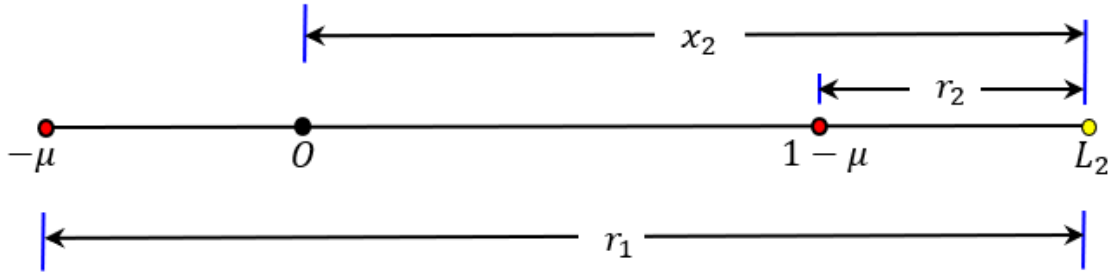

 FIGURE 1.4: Notation for computation of L_1

which simplifies to

$$\begin{aligned}
 & 2n^2\gamma^9 - 2n^2(5 - \mu)\gamma^8 + 4n^2(5 - 2\mu)\gamma^7 - 2[10n^2 - 6n^2\mu - (1 - \mu)q_1 + \mu q_2]\gamma^6 \\
 & + 2[5n^2 - 4n^2\mu - 2(1 - \mu)q_1 + 4\mu q_2]\gamma^5 \\
 & - [2(1 - \mu)(n^2 - q_1) - 3(1 - \mu)q_1A_1 + 3\mu q_2(4 + A_2)]\gamma^4 \\
 & + 4\mu q_2(2 + 3A_2)\gamma^3 - 2\mu q_2(1 + 9A_2)\gamma^2 + 12\mu q_2A_2\gamma - 3\mu q_2A_2 = 0. \tag{1.30}
 \end{aligned}$$

Solving equation (1.30) for positive real roots of γ , the location of L_1 is obtained as $(1 - \mu - \gamma, 0, 0)$.

Location of L_2


 FIGURE 1.5: Notation for computation of L_2

In this case, the Lagrangian point L_2 lies on the right side of P_2 and it is located at $(x_2, 0, 0)$. Then from Fig. 1.5,

$$r_1 = x_2 + \mu, \quad r_2 = x_2 + \mu - 1.$$

Since P_2 is the nearest primary to L_2 , we have, $r_2 = \gamma$ and

$$x_2 = 1 - \mu + \gamma, \quad r_1 = 1 + \gamma. \tag{1.31}$$

Using (1.31) in (1.26), we get

$$n^2(1 - \mu + \gamma) - \frac{(1 - \mu)q_1}{(1 + \gamma)^2} - \frac{3(1 - \mu)q_1A_1}{2(1 + \gamma)^4} - \frac{\mu q_2}{\gamma^2} - \frac{3\mu q_2A_2}{2\gamma^4} = 0$$

which simplifies to

$$\begin{aligned} & 2n^2\gamma^9 + 2n^2(5 - \mu)\gamma^8 + 4n^2(5 - 2\mu)\gamma^7 + 2[10n^2 - 6n^2\mu - (1 - \mu)q_1 - \mu q_2]\gamma^6 \\ & + 2[5n^2 - 4n^2\mu - 2(1 - \mu)q_1 - 4\mu q_2]\gamma^5 \\ & + [2(1 - \mu)(n^2 - q_1) - 3(1 - \mu)q_1A_1 - 3\mu q_2(4 + A_2)]\gamma^4 \\ & - 4\mu q_2(2 + 3A_2)\gamma^3 - 2\mu q_2(1 + 9A_2)\gamma^2 - 12\mu q_2A_2\gamma - 3\mu q_2A_2 = 0. \end{aligned} \quad (1.32)$$

Then L_2 is located at $(1 - \mu + \gamma, 0, 0)$, where γ is the positive real root of the equation (1.32).

Location of L_3

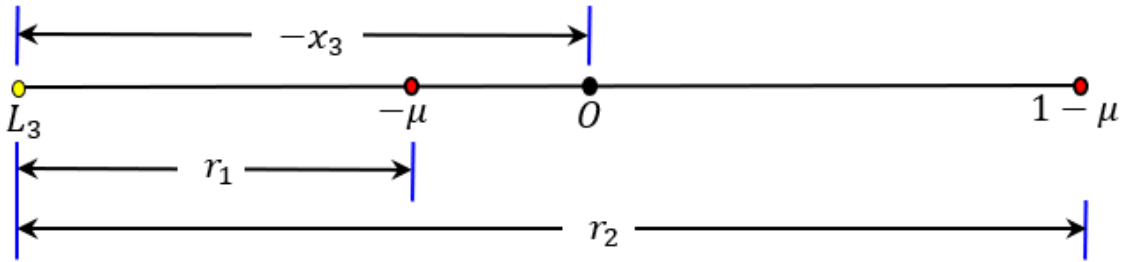


FIGURE 1.6: Notation for computation of L_3

In the case of L_3 , P_1 is the nearest primary to Lagrangian point. So, the distance between L_3 and P_1 is γ and since L_3 is located at $(x_3, 0, 0)$ and lies on the left side of the origin, the distance between the Lagrangian point L_3 and the origin O is $-x_3$. Then we have

$$r_1 = -x_3 - \mu, \quad r_2 = 1 - \mu - x_3.$$

From Fig. 1.6,

$$x_3 = -\mu - \gamma, \quad r_1 = \gamma, \quad r_2 = 1 + \gamma. \quad (1.33)$$

Using (1.33) in (1.26), we get

$$n^2(-\mu - \gamma) + \frac{(1 - \mu)q_1}{\gamma^2} + \frac{3(1 - \mu)q_1A_1}{2\gamma^4} + \frac{\mu q_2}{(1 + \gamma)^2} + \frac{3\mu q_2A_2}{2(1 + \gamma)^4} = 0$$

which simplifies to

$$\begin{aligned}
& 2n^2\gamma^9 + 2n^2(4 + \mu)\gamma^8 + 4n^2(3 + 2\mu)\gamma^7 + 2[2n^2(2 + 3\mu) - (1 - \mu)q_1 - \mu q_2]\gamma^6 \\
& - 2[4(1 - \mu)q_1 + 2\mu q_2 - n^2(1 + 4\mu)]\gamma^5 \\
& - [12(1 - \mu)q_1 + 2\mu q_2 + 3(1 - \mu)q_1 A_1 + 3\mu q_2 A_2 - 2n^2\mu]\gamma^4 \\
& - 4(1 - \mu)(2 + 3A_1)q_1\gamma^3 - 2(1 - \mu)(1 + 9A_1)q_1\gamma^2 \\
& - 12(1 - \mu)q_1 A_1\gamma - 3(1 - \mu)q_1 A_1 = 0.
\end{aligned} \tag{1.34}$$

Solving (1.34) for positive real root, the location of L_3 is obtained as $(-\mu - \gamma, 0, 0)$.

1.4.2 Computation of collinear Lagrangian points in ERTBP

Equilibrium points of system (1.24) can be computed by solving three simultaneous equations

$$\bar{\Omega}_x = 0, \quad \bar{\Omega}_y = 0, \quad \bar{\Omega}_z = 0.$$

From (1.25), we get

$$\frac{1}{\sqrt{1 - e^2}} \left[x - \frac{(1 - \mu)q_1(x + \mu)}{r_1^3} - \frac{\mu(x + \mu - 1)q_2}{r_2^3} \right] = 0, \tag{1.35}$$

$$\frac{1}{\sqrt{1 - e^2}} \left[1 - \frac{(1 - \mu)q_1}{r_1^3} - \frac{\mu q_2}{r_2^3} \right] y = 0, \tag{1.36}$$

$$\frac{1}{\sqrt{1 - e^2}} \left[\frac{(1 - \mu)q_1}{r_1^3} + \frac{\mu q_2}{r_2^3} \right] z = 0. \tag{1.37}$$

From (1.37), $z = 0$ which implies all equilibrium points are coplanar. Since collinear Lagrangian points lie on the x -axis of dimensionless synodic frame, solution of (1.35) should be obtained by considering $y = 0$ and $z = 0$. In this case also, suppose the Lagrangian point L_i is has coordinates $(x_i, 0, 0)$, $i = 1, 2, 3$ and γ is the distance between the Lagrangian point and its nearest primary.

Location of L_1

In this case also, values of x_1, r_1 and r_2 are same as given in (1.29). Using these values in (1.35), we get

$$(1 - \mu - \gamma) - \frac{(1 - \mu)q_1}{(1 - \gamma)^2} + \frac{\mu q_2}{\gamma^2} = 0$$

which simplifies to a quintic in γ given by

$$\gamma^5 - (3 - \mu)\gamma^4 + (3 - 2\mu)\gamma^3 - [\mu q_2 + (1 - \mu)(1 - q_1)]\gamma^2 + 2\mu q_2\gamma - \mu q_2 = 0. \tag{1.38}$$

Solving (1.38) for positive real root of γ , the location of L_1 is obtained as $(1 - \mu - \gamma, 0, 0)$.

Location of L_2

For L_2 , values of x_2, r_1 and r_2 are as in (1.31). Substituting these values in (1.35), we get,

$$(1 - \mu + \gamma) - \frac{(1 - \mu)q_1}{(1 + \gamma)^2} - \frac{\mu q_2}{\gamma^2} = 0.$$

Simplification leads to

$$\gamma^5 + (3 - \mu)\gamma^4 + (3 - 2\mu)\gamma^3 + [(1 - \mu)(1 - q_1) - \mu q_2]\gamma^2 - 2\mu q_2 \gamma - \mu q_2 = 0. \quad (1.39)$$

Using the positive real root γ of (1.39), location of L_2 in ERTBP can be obtained as $(1 - \mu + \gamma, 0, 0)$.

Location of L_3

For L_3 , the values of x_3, r_1 and r_2 are as in (1.33). Using these values in (1.35), we get

$$(-\mu - \gamma) + \frac{(1 - \mu)q_1}{\gamma^2} + \frac{\mu q_2}{(1 + \gamma)^2} = 0$$

which simplifies to

$$\begin{aligned} &\gamma^5 + (2 + \mu)\gamma^4 + (1 + 2\mu)\gamma^3 - [(1 - \mu)q_1 \\ &+ \mu(1 - q_2)]\gamma^2 - 2(1 - \mu)q_1\gamma - (1 - \mu)q_1 = 0. \end{aligned} \quad (1.40)$$

Then L_3 is located at $(-\mu - \gamma, 0, 0)$ and γ is the positive real root of (1.40).

1.5 Solution techniques

In this section, different methods used for finding periodic orbits in two and three dimensions are described. Lindstedt-Poincaré method is an analytical method which is useful for finding the initial state vector for planar Lyapunov orbits and three dimensional halo orbits in CRTBP and ERBP framework. The initial condition obtained using the Lindstedt-Poincaré method is revised with the help of numerical method of Differential Corrections (DC) for getting more accurate solution.

Poincaré Surface of Sections (PSS) can be used for getting the initial conditions for various planar periodic orbits. For getting a PSS, system (1.49) is solved using the Runge-Kutta-Gill method with fixed step size and the point (x, x') corresponding to each solution for which $y = 0$ and $y' > 0$ is plotted on a two-dimensional hyperspace of

four dimensional phase space. Periodic orbits give rise to fixed points that are the centre of islands of stability and islands correspond to the quasi-periodic orbits librating around the stable positions.

1.5.1 Lindstedt-Poincaré method

Systems (1.6) and (1.24) contain non-linear terms which change the frequency of the linearized system and give rise to secular terms. The terms whose amplitude grow with time are called secular terms. Lindstedt-Poincaré method is an analytical method which uses the method of perturbations for removing the secular terms appearing in the solution. For this, a new independent variable $\tau = \omega t$, where t is existing independent variable and ω , called the frequency connection term, is considered. Then the systems (1.6) and (1.24) are expressed in terms of new independent variable τ and the solutions of these systems are assumed in the perturbation form as

$$X(\tau) = \epsilon X_1(\tau) + \epsilon^2 X_2(\tau) + \epsilon^3 X_3(\tau) + \dots, \quad (1.41)$$

$$Y(\tau) = \epsilon Y_1(\tau) + \epsilon^2 Y_2(\tau) + \epsilon^3 Y_3(\tau) + \dots, \quad (1.42)$$

$$Z(\tau) = \epsilon Z_1(\tau) + \epsilon^2 Z_2(\tau) + \epsilon^3 Z_3(\tau) + \dots, \quad (1.43)$$

and

$$\omega = 1 + \epsilon \omega_1 + \epsilon^2 \omega_2 + \epsilon^3 \omega_3 + \dots. \quad (1.44)$$

Here, the aim is to select the values of ω_i , $i = 1, 2, 3, \dots$, in such a manner that terms giving rise to secular terms are avoided from the equations of motion. To accomplish this aim, the solutions (1.41)-(1.44) are substituted in the systems (1.6) and (1.24) and the coefficients of n^{th} powers of ϵ are equated to get the n^{th} order approximate solution, $n = 1, 2, 3, \dots$. Usually, the series in equations (1.41)-(1.44) are terminated after three or four or five terms giving the third or fourth or fifth order approximate solution. Computation of halo orbits using Lindstedt-Poincaré method is described in detail in Chapter 2 for CRTBP framework and in Chapter 4 for ERTBP framework.

1.5.2 Differential Correction method

The numerical method of differential corrections (DC) or multi-dimensional Newton-Raphson's method is useful for modifying the state vectors of trajectories having certain constraints. Halo orbits are three dimensional periodic orbits which are symmetric about xz plane and intersect this plane perpendicularly. This characteristic makes the computation of halo orbits similar to solving a two point boundary value problem. In DC method, design variables are modified in such a manner that all given constraints

are satisfied simultaneously. Suppose

$$\mathbf{X} = \begin{bmatrix} X_1 \\ X_2 \\ \vdots \\ X_n \end{bmatrix}$$

is a free variable vector with n independent design variables X_1, X_2, \dots, X_n . In most of the cases, \mathbf{X} contains the elements of state vector and integration time. The design variables can be modified subject to m scalar constraint equations

$$\mathbf{F}(\mathbf{X}) = \begin{bmatrix} F_1(\mathbf{X}) \\ F_2(\mathbf{X}) \\ \vdots \\ F_m(\mathbf{X}) \end{bmatrix} = \mathbf{0}.$$

In most of the cases, constraints are position, time of flight and velocity. Consider an initial guess \mathbf{X}^0 for determining a free variable vector \mathbf{X}^* such that $\mathbf{F}(\mathbf{X}^*) = \mathbf{0}$. Expanding the constraint vector in a Taylor series about initial guess \mathbf{X}^0 ,

$$\mathbf{F}(\mathbf{X}) = \mathbf{F}(\mathbf{X}^0) + \frac{\partial \mathbf{F}(\mathbf{X}^0)}{\partial \mathbf{X}^0}(\mathbf{X} - \mathbf{X}^0) + \dots$$

Now, denoting $\partial \mathbf{F}(\mathbf{X}^0)/\partial \mathbf{X}^0$, an $m \times n$ Jacobian matrix of partial derivatives of constraint vector as $D\mathbf{F}(\mathbf{X}^0)$ and truncating the Taylor series to first order gives

$$\mathbf{F}(\mathbf{X}) = \mathbf{F}(\mathbf{X}^0) + D\mathbf{F}(\mathbf{X}^0)(\mathbf{X} - \mathbf{X}^0). \quad (1.45)$$

Since for a solution $\mathbf{F}(\mathbf{X}) = \mathbf{0}$, equation (1.45) in an iterative update form can be written as

$$\mathbf{F}(\mathbf{X}^j) + D\mathbf{F}(\mathbf{X}^j)(\mathbf{X}^{j+1} - \mathbf{X}^j) = \mathbf{0} \quad (1.46)$$

where \mathbf{X}^j is the current iteration of the free variable vector, \mathbf{X}^{j+1} is the next iteration of the free variable vector, and $\mathbf{F}(\mathbf{X}^j)$ is the value of the current constraint vector as evaluated after propagating the equations of motion from the initial condition \mathbf{X}^j . The value of $D\mathbf{F}(\mathbf{X}^j)$ can be obtained with the help of \mathbf{X}^j and $\mathbf{F}(\mathbf{X}^j)$. Equation (1.46) represented in the form

$$\mathbf{X}^{j+1} = \mathbf{X}^j - D\mathbf{F}(\mathbf{X}^j)^{-1}\mathbf{F}(\mathbf{X}^j) \quad (1.47)$$

is used as an update equation until $\|\mathbf{F}(\mathbf{X}^{j+1})\|_2 < 10^{-12}$. In most of the cases, desired accuracy is reached within 10 iterations.

The initial state vector of halo orbit obtained using the Lindstedt-Poincaré method is modified using the DC method. Since halo orbits are symmetric about xz plane, we must have $y = 0$ at half period and also, these orbits intersect xz plane perpendicularly so at half period, we must have $\dot{x} = \dot{z} = 0$. Then the free variable vector for revising the state vector of halo orbit is

$$\mathbf{X} = \begin{bmatrix} x \\ \dot{y} \\ T/2 \end{bmatrix}$$

and the constraint vector is

$$\mathbf{F}(\mathbf{X}) = \begin{bmatrix} y \\ \dot{x} \\ \dot{z} \end{bmatrix} = \mathbf{0}$$

with the Jacobian matrix

$$D\mathbf{F}(\mathbf{X}) = \begin{bmatrix} O & I_3 \\ \mathcal{U} & K \end{bmatrix},$$

where

$$\mathcal{U} = \begin{bmatrix} \Omega_{xx} & \Omega_{xy} & \Omega_{xz} \\ \Omega_{yx} & \Omega_{yy} & \Omega_{yz} \\ \Omega_{zx} & \Omega_{zy} & \Omega_{zz} \end{bmatrix}, \quad K = \begin{bmatrix} 0 & 2 & 0 \\ -2 & 0 & 0 \\ 0 & 0 & 0 \end{bmatrix}, \quad (1.48)$$

and Ω is pseudo potential, the matrix O is 3×3 null matrix and I_3 is 3×3 identity matrix. Here, (x, y, z) is position vector, $(\dot{x}, \dot{y}, \dot{z})$ is velocity vector and T is period of halo orbit. In this case, the z coordinate of the position vector is not considered in the free variable vector so its value will remain unchanged throughout the correction scheme. Further, it is possible to keep x coordinate of position vector fixed by removing it from the free variable vector and inserting z coordinate instead.

1.5.3 Runge-Kutta-Gill method

Runge-Kutta-Gill (RKG) method is a numerical method useful for solving first order Initial Value Problems (IVPs) numerically. The algorithm for solving an autonomous IVP consisting m ODEs using RKG method with fixed step size is given below:

Consider the Initial Value Problem containing m ODEs

$$y'_j = \frac{dy_j}{dx} = f_j(y_1, y_2, y_3, \dots, y_m), \quad y_j(x_0) = y_j^0, \quad j = 1, 2, \dots, m.$$

1. Select the step size h .
2. Find the quantity: $k_j^1 = hf_j(y_1^i, y_2^i, y_3^i, \dots, y_m^i)$.
3. Update y_j^i as $y_j^{i,1} = y_j^i + 0.5k_j^1$.
4. Calculate k_j^2 as $k_j^2 = hf_j(y_1^{i,1}, y_2^{i,1}, y_3^{i,1}, \dots, y_m^{i,1})$.
5. Further update y_j^i as $y_j^{i,2} = y_j^{i,1} + 0.5k_j^1(-1 + \sqrt{2}) + k_j^2(1 - 0.5\sqrt{2})$.
6. Compute the quantity: $k_j^3 = hf_j(y_j^{i,2}, y_2^{i,2}, y_3^{i,2}, \dots, y_m^{i,2})$.
7. Update y_j^i as $y_j^{i,3} = y_j^{i,2} - \left[\frac{k_j^2}{\sqrt{2}} + (1 + \frac{1}{\sqrt{2}})k_j^3 \right]$.
8. Evaluate the quantity: $k_j^4 = hf_j(y_1^{i,3}, y_2^{i,3}, y_3^{i,3}, \dots, y_m^{i,3})$.
9. Then, the new iterate of y_j^i, y_j^{i+1} , can be obtained as

$$y_j^{i+1} = y_j^{i,3} + \frac{1}{6}[k_j^1 + (2 - \sqrt{2})k_j^2 + (2 + \sqrt{2})k_j^3 + k_j^4], \quad i \geq 0.$$

This process is repeated till the desired accuracy is obtained. Our aim is to obtain periodic orbits in planar ERTBP by considering the more massive primary as a source of radiation. In this case, we shall denote q_1 by q , the mass reduction factor of the second primary, $q_2 = 1$ and system (1.24) gets transformed to

$$\begin{aligned} x'' - 2y' &= \frac{\partial \bar{\Omega}}{\partial x}, \\ y'' + 2x' &= \frac{\partial \bar{\Omega}}{\partial y}, \end{aligned} \tag{1.49}$$

where

$$\begin{aligned} \bar{\Omega} &= \frac{1}{\sqrt{1-e^2}} \left[\frac{1}{2}(x^2 + y^2) + \frac{(1-\mu)q}{r_1} + \frac{\mu}{r_2} \right], \\ r_1 &= \sqrt{(x+\mu)^2 + y^2}, \\ r_2 &= \sqrt{(x+\mu-1)^2 + y^2}. \end{aligned} \tag{1.50}$$

Since system (1.49) contains second order differential equations, it is converted into equivalent first order system and then RKG method is applied to a system of four first order equations with step size $h = 0.001$.

1.5.4 Poincaré Surface of Sections

The study of a complex dynamical system can be simplified by reducing its dimension. Poincaré map is one such useful tool which effectively reduces the dimension of the dynamical system and converts a continuous system into a corresponding discrete system. The technique of Poincaré map was introduced by Henri Poincaré in 1881 in which the crossing of a trajectory to a particular hyperplane is recorded. First, a particular value of Jacobi constant or energy constant is selected for the numerical propagation. RKG method with fixed step size is used commonly for numerical propagation of system (1.49). Jacobi constant is given by

$$C = \frac{1}{\sqrt{1-e^2}} \left[x^2 + y^2 + \frac{2(1-\mu)q}{r_1} + \frac{2\mu}{r_2} \right] - x'^2 - y'^2. \quad (1.51)$$

Equation (1.51) shows selecting a particular value of C reduces the degree of freedom and hence the orbits will lie in three dimensional subspace $C(x, y, x', y') = C$ embedded in a four dimensional phase space. Further, by specifying a hyperplane, three dimensional subspace is projected onto a two dimensional (x, x') plane (Murray and Dermott (1999)). In most of the cases, the plane $y = 0$ is considered as hyperplane and it is further assumed that at initial time, the infinitesimal body lies on the x axis and there is no velocity in the x direction. Then the velocity in the y direction can be obtained from

$$y' = \sqrt{\frac{1}{\sqrt{1-e^2}} \left(x^2 + \frac{2(1-\mu)q}{r_1} + \frac{2\mu}{r_2} \right) - C}. \quad (1.52)$$

The equations (1.51) and (1.52) corresponding to CRTBP can be obtained by putting $e = 0$.

1.6 Objective of present works

There are two major objectives of present works: The first objective is to refine and modify the existing technique of obtaining halo orbits to do more precise orbit determination. For this purpose, the existing fourth order Lindstedt-Poincaré approximate solution in CRTBP framework is extended to fifth order approximate solution. The separation between the third and fourth, and fourth and fifth order solutions decrease which shows as the order of the solution increases, more accurate solution is obtained. The fifth order approximate solution is used to study the effects of mass factor of primaries on various parameters of halo orbits. The second objective is to extend the method of Poincaré Surface of Sections from CRTBP to ERTBP and compute different planar resonant periodic orbits in ERTBP framework. With the help of PSS, f -family

orbits and first order interior as well as exterior resonant orbits in Sun-Saturn ERTBP are computed, and effects of eccentricity of primaries' orbit on parameters of resonant periodic orbits are analyzed.

1.7 Organization of Thesis

This thesis is divided into eight chapters. **Chapter 1** is introduction in which the motivation for the study and different mathematical tools and techniques used in the study of CRTBP and ERTBP are presented. At the end, summary of subsequent chapters is given.

In Chapter 2, computation of halo orbits around L_1, L_2 and L_3 using the analytic and numerical method in CRTBP framework is given. By considering the perturbation due to radiation pressure and oblateness of both the primaries, analytic solution for computing halo orbits upto fifth order approximation using Lindstedt-Poincaré technique is obtained. Using this analytic solution as a first guess in DC scheme, halo orbits around L_1 and L_2 of the Sun-Earth system are computed numerically for different solar radiation pressure and oblateness of Earth. Also, the third and fourth order analytical solutions were used for finding halo orbits for analyzing the accuracy of the solutions. It was observed that the separation between halo orbit decreases as the order of solution increases. So, fifth order initial solution provides more precise initial guess than third or fourth order solution.

Further, the effects of perturbing forces due to radiation pressure and oblateness on location, size, period, frequency correction term and other parameters of halo orbits around L_1, L_2 and L_3 are studied. (Tiwary and Kushvah (2015)) computed fourth order analytic solution for halo orbits in the photogravitational Sun-Earth CRTBP with oblateness. Variation in parameters of halo orbits around L_1 and L_2 due to variation in q_1 and A_2 was similar to observations of Tiwary and Kushvah (2015). Due to increase in solar radiation pressure, halo orbits around L_3 shrink and move towards the more massive primary. Further, period of these orbits decrease. Oblateness of second primary shifts orbits around L_3 towards the more massive primary and decreases period. To study the effect of oblateness of more massive primary on halo orbits around L_1 and L_2 , the Earth-Moon system with actual oblateness of the Earth is considered. It is observed that due to increase in A_1 , halo orbits around L_1 and L_2 both elongate and move towards the second primary, and period decreases. Radiation pressure of second primary shrinks halo orbits around L_1 and enlarges halo orbits around L_2 . A decrease in q_2 shifts orbits around L_1 towards m_2 and orbits around L_2 towards m_1 , and period of orbits around L_1 increase while around L_2 decreases.

Chapter 3 analyzes the effects of mass ratio $\mu = m_2/(m_1 + m_2)$ on parameters of halo orbits around L_1, L_2 and L_3 in CRTBP framework. Different random values of μ in the interval $[10^{-8}, 0.5]$ are considered. Starting with 10^{-8} , value of μ is increased with a fixed step size of 10^{-6} until $\mu = 0.5$. It is observed that as the value of μ increases, Lagrangian point L_1 and halo orbits around it shift towards the more massive primary while Lagrangian point L_2 and corresponding halo orbits recede from second primary till $\mu_0 = 0.17894$ and for $\mu > \mu_0$, orbits move towards the second primary. For verifying these results, Sun-Mars, Sun-Earth, Sun-Earth+Moon, Sun-Saturn and Sun-Jupiter systems are considered and halo orbits around all three collinear Lagrangian points are computed. It is observed that as the value of μ increases, Lagrangian point L_3 and corresponding orbits move towards the more massive primary. Suppose A_x, A_y and A_z represent the amplitudes of halo orbits in the x, y and z direction, respectively. For a halo orbit, A_y is a multiple of A_x , and A_x and A_z are related by amplitude constraint, it is enough to study the variation in either A_x or A_z . For $A_z = 3.25 \times 10^{-4}$, corresponding value of A_x is obtained using amplitude constraint relation for $\mu \in [10^{-8}, 0.5]$. It is found that μ and A_x are inversely proportional for orbits around L_1 while they are directly proportional for orbits around L_2 . For analyzing the variation in amplitude of halo orbits around L_3 , $A_x = 0.045$ was considered for finding corresponding A_z value. Study shows that A_z increases with the increase in μ . Period of halo orbits around L_1 and L_3 decreases while it increases for orbits around L_2 with the increase in μ . The size, initial distance from origin and initial velocity of orbits are also affected by the value of μ . The analysis shows orbits around L_1 and L_2 both elongate as μ increases. Further, with the increase in the value of μ , halo orbits around L_1 come close to the origin and orbits around L_2 move away from the origin. The initial velocity of spacecraft in orbits around L_1 as well as L_2 increase with the increase in mass ratio.

In Chapter 4, computation of halo orbits around L_1, L_2 and L_3 in the photogravitational Sun-Mars ERTBP is given. Szebehely (1967) has discussed the motion of an infinitesimal body in a dimensionless synodic pulsating coordinate system in ERTBP framework which is a non-autonomous system with true anomaly as independent variable. This non-autonomous system has been converted into an autonomous system by averaging the system with respect to new independent variable as the eccentric anomaly E of the second primary. Computation of locations of collinear equilibrium points in this system shows that due to solar radiation pressure, location of equilibrium points vary. The location of Lagrangian points do not change with the change in the eccentricity of the orbit of the primaries. Computation of the third order approximate solution using Lindstedt-Poincaré method is described and the procedure of finding halo orbits using differential correction method is given. Monodromy matrix is the

State Transition Matrix (STM) evaluated at one period of halo orbit. The eigenvalues of monodromy matrix are used for analyzing the stability of periodic orbits and finding bifurcations. If λ_i ($i = 1, 2, \dots, 6$) are eigenvalues of monodromy matrix, then the stability index is defined as $\nu_i = (\lambda_i + 1/\lambda_i)/2$. Since eigenvalues of monodromy matrix are always in reciprocal pairs, there are three stability indices corresponding to a periodic orbit. Further, two eigen values of monodromy matrix are always unity and hence the stability index, say ν_2 , corresponding to this pair is always unity (Zimovan (2017)). Halo orbits are obtained as tangent bifurcation from planar Lyapunov orbits when the out-of-plane stability index ν_3 crosses the line $\nu_3 = 1$. A periodic orbit is stable if all stability indices have value between -1 and 1 (Vutukuri (2018)). Due to solar radiation pressure of the Sun, the separation between the halo and axial bifurcation increases. This holds true for orbits around L_1 and L_2 both. Halo orbits around L_1 shrink, move towards the Sun and periods of orbits increase due to increase in solar radiation pressure. But orbits around L_2 enlarge, move towards the Sun and their periods decrease due to increases in solar radiation pressure. The effect of solar radiation pressure on halo orbits around L_1 and L_3 were found to be similar. A graphical comparison of size of halo orbits show that due to non-zero eccentricity of the orbit of the primaries, halo orbits shrink.

Chapter 5 contains evolution of f -family orbits in the photogravitational Sun-Saturn ERTBP framework. The technique of PSS is extended from CRTBP to ERTBP for exploring periodic orbits. Variations in parameters of f -family orbits due to variation in eccentricity of the orbit of the primaries, solar radiation pressure and Jacobi constant are observed. The existence of energy integral puts a constraint on the value of Jacobi constant. So, it is necessary to find the maximum value of C , say C_M , corresponding to each pair (q, e) such that for $C \leq C_M$, $v^2 \geq 0$, where v is the velocity of the infinitesimal body. For $e \in [0, 0.1]$ and $q = 0.98, 0.99$ and 1 computation of C_M shows that a quadratic polynomial in e provides the curve of best fit for approximating C_M for $q = 0.98, 0.99$ and 1. Further, it has been observed that the excluded region shifts towards the second primary due to increase in eccentricity of orbit of the primaries. Analysis shows f -family orbits shift towards the more massive primary and their diameters and periods increase with an increase in the value of e . An increase in solar radiation pressure decreases the value of C_M and expands the excluded region of motion for a satellite. Regression analysis shows that the functional relation between the length of excluded region and e depends on solar radiation pressure of the Sun as well. Since solar radiation pressure is a repulsive force, orbits move towards the second primary and their diameter decreases. Due to perturbing force of solar radiation pressure, the value of C and the difference of energy levels at separatrices decreases

and variation in size and shape of islands and f -family orbits is also observed. By considering different values of Jacobi constant C in the interval $[2.77, 3.017]$, variations in parameters of f -family orbits are analyzed and the results agree with Pathak and Thomas (2016) for CRTBP framework.

Chapter 6 is devoted to the study of first order exterior resonant periodic orbits in the photogravitational Sun-Saturn ERTBP framework. Using the numerical technique of PSS, 1:2, 2:3, 3:4, 4:5 and 5:6 resonant periodic orbits are obtained and the effects of eccentricity of the orbit of the primaries (e), solar radiation pressure (q) and Jacobi constant (C) on location, period, eccentricity (e_s) and semi-major axis (a_s) of these periodic orbits are studied. For an exterior resonance, in the ratio $p : p + s$, p denotes number of loops in the orbit of a spacecraft and s denotes the order of resonance. It is observed that the first order exterior resonant orbits lie on the right side of f -family orbits. For observing the effects of variation in e on parameters of resonant periodic orbits, e is varied in the interval $[0, 0.1]$. The observations show that the orbits move towards the Sun due to increase in the value of e . Further, an increase in period and a decrease in semi-major axis of orbits is observed due to non-zero value of e . The variation in e_s is not similar for all orbits. The eccentricity e_s of 1 : 2 resonant orbits decreases with the increase in e while e_s increases with the increase in e for $p : p + 1$, $p \in \{2, 3, 4, 5\}$ resonant orbits. Effects of solar radiation pressure and Jacobi constant are similar in CRTBP and ERTBP framework.

In Chapter 7, analysis of first order interior resonant orbits is performed. These orbits lie on the left side of f -family orbits. In this case, the resonance ratio is of the form $p + s : p$ in which s denotes the order of resonance and $p + s$ denotes the number of loops in the orbit of spacecraft. The number of islands corresponding to a $p + s : p$ resonant orbit denotes the order of resonance. For distinct values of $e \in [0, 0.09]$, 2:1, 3:2, 4:3 and 5:4 resonant periodic orbits are computed. The study shows that these orbits recede from the Saturn and advance towards the Sun. Further, with the increase in e , the period, semi-major axis (a_s) and eccentricity (e_s) of these orbits increase. The analysis of size and shape of these orbits reveals that orbits shrink while their loops enlarge due to increment in the value of e . Due to solar radiation pressure, orbits advance towards the Saturn and period, semi-major axis (a_s) and eccentricity (e_s) decrease. Further, orbits enlarge while the loops of these orbits shrink due to solar radiation pressure. By considering five different values of Jacobi constant in the interval $[2.88, 2.92]$, the effects of Jacobi constant C on parameters of resonant orbits are analyzed.

Chapter 8 contains conclusions and a brief overview of future scopes for research in

this field and is followed by list of publications and bibliography. Lengthy expressions involved in Chapter 2 and Chapter 4 are given in Appendices A and B, respectively.